Appl Phys A (2008) 92: 749–753
DOI 10.1007/s00339-008-4584-1

Applied Physics A
Materials Science & Processing

Material processing of dielectrics with temporally asymmetric shaped femtosecond laser pulses on the nanometer scale

L. Englert · M. Wollenhaupt · L. Haag · C. Sarpe-Tudoran · B. Rethfeld · T. Baumert

Received: 12 October 2007 / Accepted: 4 March 2008 / Published online: 22 May 2008

Abstract Laser material processing of dielectrics with temporally asymmetric femtosecond laser pulses of identical fluence, spectrum, and statistical pulse duration is investigated experimentally. To that end single shot structures at the surface of fused silica as a function of fluence and pulse shape are analyzed with the help of scanning electron microscopy. Structures for the bandwidth limited pulses show the known expansion in structure size with increasing laser fluence approaching the diffraction limit, which is 1.4 µm for the 0.5NA microscope objective used. In contrast, structures from the asymmetric pulses are remarkably stable with respect to variations in laser fluence and stay below 300 nm despite doubling the fluence. Different thresholds for surface material modification with respect to an asymmetric pulse and its time reversed counterpart are attributed to control of different ionization processes.

PACS 78.47.-p · 81.16.-c · 42.62.-b

1 Introduction

Ultrashort laser pulses have emerged as a powerful tool for processing dielectrics ranging from industrial precision micro machining to life science [1–5]. As dielectrics are mainly transparent for visible and near infrared light, an alteration of the material is mainly evoked by nonlinear processes requiring high intensities available via ultrashort laser pulses. Investigated material modifications include refractive index changes, ablation, void creation, and filamentation. Recent experiments on laser ablation show a strong dependence on pulse duration [6–8]. The temporal profile of the pulses has as well a strong influence on laser induced damage, demonstrated in double pulse experiments [9–11] and symmetric pulse sequence experiments [12] making use of sinusoidal phase modulation [13] in a spatial light modulator for femtosecond pulse shaping [14]. In this contribution we present our experiments on laser surface damage on fused silica with temporally asymmetric shaped femtosecond laser pulses obtained by introducing third-order dispersion (TOD) via spectral phase modulation in our home built pulse shaper [15]. Analytic formulas for cubic phase shaped laser pulses of the form $\phi(\omega) = \frac{\phi_3}{3!}(\omega - \omega_0)^3$, where ϕ_3 is termed TOD and ω_0 is the central frequency, can be found in [16, 17]. We first describe our experimental set-up for material processing and determine surface structure diameters and energy thresholds with the help of post mortem scanning electron microscopy (SEM) before we discuss the obtained results.

2 Experimental setup

The experimental setup is shown in Fig. 1. Linear polarized laser pulses with 35 fs full width at half maximum (FWHM) pulse duration and a central wavelength of 790 nm are provided by an amplified Ti:Sapphire laser system (Femtolasers Femtopower Pro). The pulses are split into two beams using a Mach–Zehnder interferometer. The first arm includes our calibrated home built spectral phase modulator, while the second arm contains a stepper motor driven delay stage used

L. Englert · M. Wollenhaupt · L. Haag · C. Sarpe-Tudoran · T. Baumert (✉)
Institut fuer Physik und CINSaT, Universitaet Kassel, Heinrich-Plett-Strasse 40, 34132 Kassel, Germany
e-mail: tbaumert@physik.uni-kassel.de

B. Rethfeld
Fachbereich Physik, Technische Universitaet Kaiserslautern, Erwin-Schroedinger-Strasse 46, 67663 Kaiserslautern, Germany

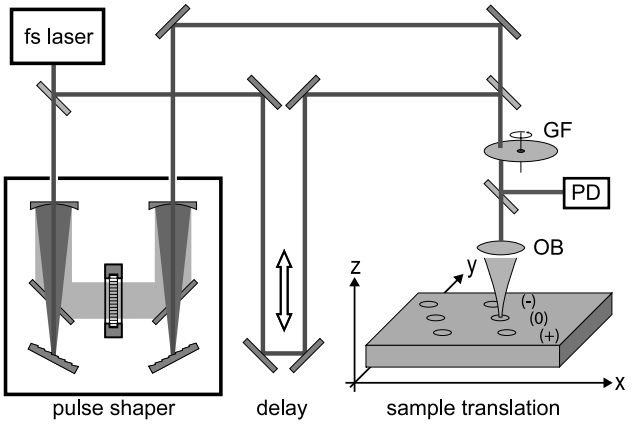

Fig. 1 Experimental setup: The femtosecond laser beam is aligned into a Mach–Zehnder interferometer. The first arm includes a spectral phase modulator, while the second arm contains a delay stage. Energy is controlled by a motorized neutral density gradient filter (GF) and monitored with a photodiode (PD). A microscope objective (OB) focuses the beam on the dielectric sample. Sample translation is done by a 3-axis piezo table

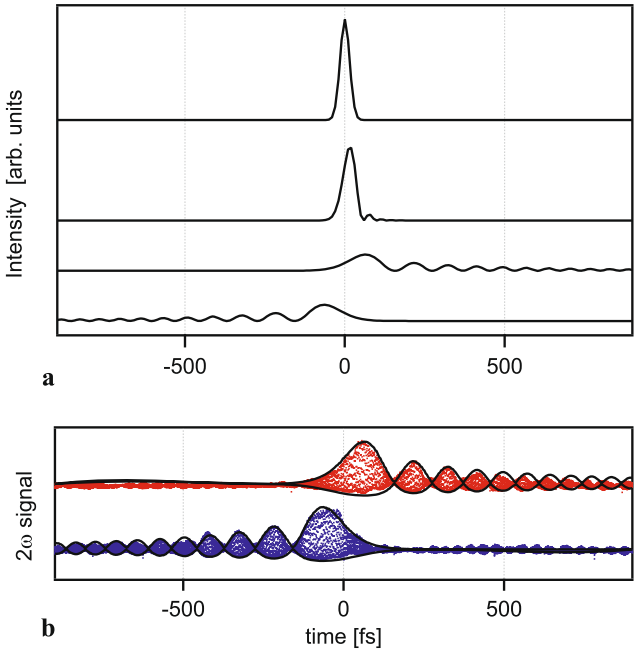

Fig. 2 (**a**) Calculated temporal intensity envelopes of pulses (*from top to bottom*) for different third order dispersions ϕ_3 (=TOD): bandwidth limited pulse ($\phi_3 = 0$ fs^3); $\phi_3 = +25 \times 10^3$ fs^3; $\phi_3 = +6 \times 10^5$ fs^3 and $\phi_3 = -6 \times 10^5$ fs^3. Relative scaling between intensities is maintained. (**b**) *Colored points*: Crosscorrelations of unmodulated and modulated ($\phi_3 = \pm 6 \times 10^5$ fs^3) pulses. *Black line*: calculated envelope

for pulse characterization, e.g., autocorrelation and crosscorrelation measurements.

After the interferometer the pulses are focused via a Zeiss Epiplan 50x/0.5NA objective to a lateral spot diameter of 1.4 µm. This calculated [18] $1/e^2$ intensity profile diameter of the point spread function was approached with 35 fs pulses in dielectrics of a fluence four times above threshold. The calculated axial spot size in air is 9.1 µm. The prism compressor in the laser system is adjusted to precompensate the dispersion in the subsequent beam path, ensured by placing a two-photon photodiode in the interaction region and performing 2nd order autocorrelations. In addition, we check for correct dispersion compensation by variation of 2nd and 3rd order spectral phase resulting in a maximal two-photon signal for a flat phase with the delay line blocked. Shaped pulses are characterized via their implemented phase functions and checked via direct crosscorrelation measurements. While phase modulation does not change the spectrum of the pulse, the temporal profile will be altered. By applying TOD we obtain pulses with an asymmetric profile in time consisting of a train of pulses (see Fig. 2). Changing the sign of the TOD inverts the time profile, while increasing the TOD stretches the pulses in time. The instantaneous frequency remains unchanged.

For material processing, phase shaped femtosecond pulses (only using the first arm of the interferometer) are focused onto the sample (fused silica, Heraeus Suprasil 2, $\lambda/10$ flatness). Single pulses are selected by the Pockels cell in the laser amplifier. The energy is adjusted via a motor driven gradient neutral density filter, and single shot pulse energies are recorded by an amplified photodiode calibrated to various commercial powermeters. The sample is translated by a 3-axis piezo table to a new position for each shot. Constant z-positioning is assured by confocal probing of the sample surface with a Helium-Neon Laser prior to material processing (not shown in Fig. 1). A typical measurement pattern consists of an array of points where we vary energy, focal z-position and TOD (see Fig. 3). For each pattern, one TOD ranging from $\phi_3 = \pm 2.5 \times 10^4$ fs^3 to $\phi_3 = \pm 6 \times 10^5$ fs^3 was chosen. Energy was increased in the horizontal direction in steps of 6 nJ, allowing observation of changes in damage threshold and structure size. The focal position was varied in the vertical direction in steps of 1 µm from 10 µm below to 10 µm above the focus obtained by the confocal scan. By this we assure having the focus in the sample surface plane and we are able to observe structural changes due to focus variations. Translation of the sample, adjusting pulse energy, applying phase masks, and single-shot control of the laser are controlled by a computer. The samples are cleaned chemically after laser processing and coated with platinum for post mortem SEM analysis. The structure sizes and thresholds for material processing are determined visually from the SEM images.

3 Results and discussion

Figure 3 shows SEM micrographs of damage structures on fused silica. A triplet of applied laser pulses with different

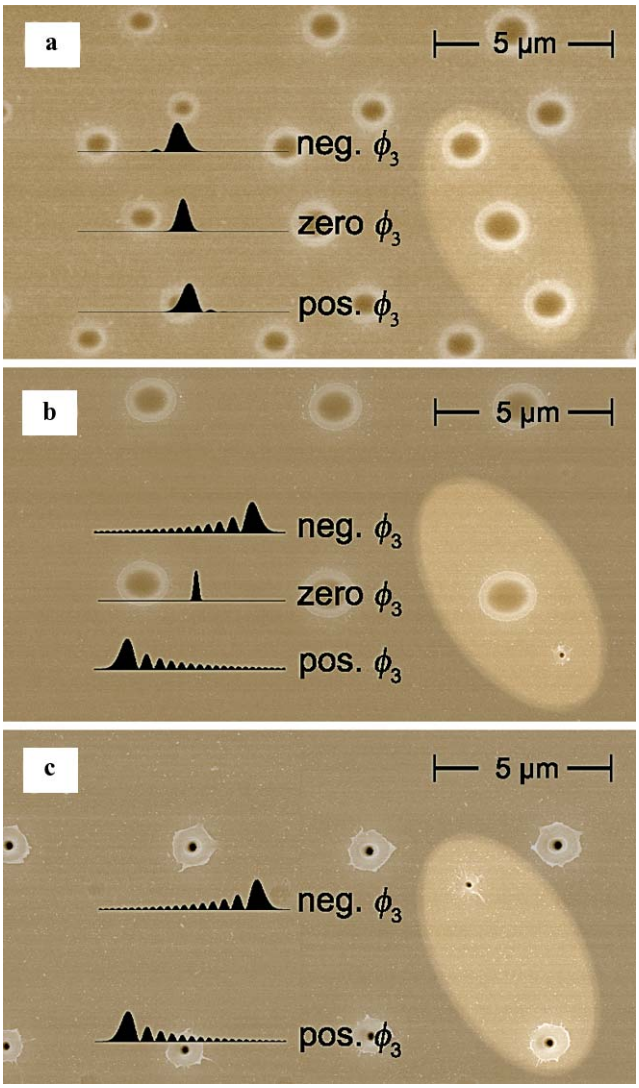

Fig. 3 Scanning electron microscope micrographs of a measurement pattern on fused silica: For an applied energy and focal position, a triplet of applied laser pulses is highlighted by the ellipse. Negative, zero, and positive TOD were used. Normalized temporal intensity profiles are sketched for comparison between different TODs. (**a**) Low TOD ($\phi_3 = \pm 2.5 \times 10^4$ fs^3, $E = 77$ nJ) results in negligible differences between created structures. (**b**) High positive TOD ($\phi_3 = +6 \times 10^5$ fs^3, $E = 71$ nJ) results in a change of structure size and threshold energy. The threshold energy for ablation with negative TOD ($\phi_3 = +6 \times 10^5$ fs^3) is reached in (**c**) with $E = 110$ nJ. Here the unshaped pulse is suppressed in order not to mask structures with TOD

TODs (negative ϕ_3, zero ϕ_3, and positive ϕ_3) for an applied energy and focal position is highlighted. For all ϕ_3, the pulses have the same energy, spectral intensity, and spatial profile. The positive and negative phase mask have the same pulse duration but their time profile is time-inverted. Figure 3a shows structures resulting from a weak TOD of $\phi_3 = \pm 2.5 \times 10^4$ fs^3 leading to no significant changes neither to the diameter nor to threshold (not shown) for material processing. The statistic pulse duration of $2\sigma = 50$ fs

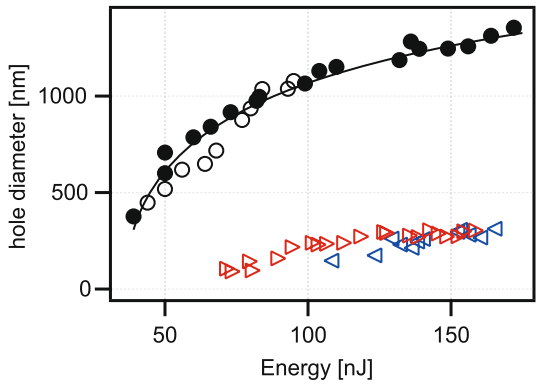

Fig. 4 Diameters of ablation structures for fused silica with $\phi_3 = 0$ fs^3 (○ and ● for two completely independent measurements confirm the reproducibility of our setup), for $\phi_3 = 6 \times 10^5$ fs^3 (▷) and $\phi_3 = -6 \times 10^5$ fs^3 (◁). *Solid line*: fit through data (see text)

is only slightly longer compared to the bandwidth limited pulse of 35 fs. For a strong TOD of $\phi_3 = \pm 6 \times 10^5$ fs^3 (see Fig. 3b), the statistic pulse length raises to $2\sigma = 960$ fs. The highlighted triplet is at the threshold energy (71 nJ) for material processing with positive ϕ_3. For $\phi_3 = -6 \times 10^5$ fs^3, the first structures appear at 110 nJ (Fig. 3c) and look similar to the structures for positive ϕ_3. In this pulse energy region, unshaped pulses are suppressed in order not to mask structures with TOD. The energies are measured single shot for the specified holes. Note within that context that the energy transmission through the phasemodulator for positive and negative TOD measured at the entrance pupil of the objective is constant and for maximum applied values up to 20% less than for bandwidth limited pulses due to scattering processes in the phasemodulator. The dependence of structure diameter with respect to energy for $\phi_3 = 0$ fs^3 and $\phi_3 = \pm 6 \times 10^5$ fs^3 is shown in Fig. 4. The diameters are taken for the holes (darker area) not covering the rim zone. Occasional crosschecks are performed with an atomic force microscope and are in agreement with the SEM data [19]. Structures for the bandwidth limited pulses show the known expansion in structure size with increasing laser fluence (see Fig. 4). The corresponding fit through the data was obtained by using the formalism presented in [20]. However, the structure sizes of both positive and negative ϕ_3 are significantly smaller than for unshaped pulses at their threshold. In addition, the increase of structure size with increasing laser energy is significantly smaller in comparison to the bandwidth limited pulses. Without changing the focus spot diameter of 1.4 µm structures below 300 nm are obtained over a large energy range thus providing a large process window for creation of nanostructures. The smallest structures are one order of magnitude below the diffraction limit. Note that even smaller structures have been reported at the backside surface of dielectric samples by using higher NA immersion objectives [21, 22]. Good reproducibility of the

nanostructures can be seen in the lower line of Fig. 3c for positive ϕ_3. Note also the different damage thresholds for positive and negative TOD. The different damage thresholds for negative and positive cubic phase masks can be explained by taking two basic ionization processes into account. A detailed discussion on this topic is given elsewhere [19], and only a short summary will be given here: a commonly accepted prerequisite for ablation is the generation of a certain critical electron density. Direct experimental studies devoted to the transient electron density are reported in [4, 23–25]. Two main processes for generating free electrons are Multiphoton-Ionization (MPI) and Avalanche-Ionization (AI). MPI requires no free initial free electrons and has highest efficiency for shortest pulses i.e., highest intensities, as it scales with I^n when n is the number of photons needed to overcome the band gap. AI on the other hand needs initial free electrons and needs time to establish. Simulations based on the multiple rate model [26] reveal that, for pulses without modulation ($\phi_3 = 0$ fs^3), an important strong field ionization effect is MPI also in accordance with [24]. At energies reaching the surface breakdown threshold also Zener ionization is discussed as a strong field ionization mechanism [21]. For $\phi_3 > 0$, a strong pulse is followed by weaker pulses. When distributing the intensity from the main pulse to some consecutive pulses (see Fig. 2a), the amount of free electrons created by the first strong pulse via MPI is not sufficient for reaching the critical electron density. However, the consecutive pulses can increase the electron density via AI to the critical density. For $\phi_3 < 0$, the intensity of the pulses increases and is terminated by a strong pulse. The first weak pulses are not intense enough for efficient MPI, and due to the absence of free electrons, also an increase of the free electron density due to AI is not operative. Only the final pulse(s) is (are) able to deliver free electrons via MPI further increased by AI during the trailing part of the final pulse. For this case, a higher energy is needed in comparison to $\phi_3 > 0$ in order to reach the critical density. In this sense, we can control the two ionization processes by employing temporally asymmetric pulse shapes. Note that the intensity maximum of an unshaped laser pulse is approximately six times higher in comparison to the intensity maxima of the pulse trains obtained with $\phi_3 = \pm 6 \times 10^5$ fs^3 at the same overall pulse energy (see Fig. 2). If only the strongest pulse in the pulse trains would be considered to be responsible for reaching the critical electron density in the same fashion as the bandwidth limited pulse does, then a sixfold increase in threshold energy would be expected. However, taking the damage threshold fluence of the bandwidth limited pulse for reference, the roughly two fold and three fold increase in threshold fluence for positive and negative TOD seen in Fig. 4 demonstrates that the sketched interplay between the ionization mechanisms is at play and that it is MPI that dominates the strong field ionization [24].

For the observed reduction of structure size for modulated pulses, the spatial electron density together with propagation effects has to be taken into account with a special emphasis on filamentation processes. We propose that it is again the interplay of MPI creating free electrons in a spatially very confined region followed by AI that restricts the area of reaching the critical electron density that may eventually lead to the filamentation like structures seen for positive and negative TOD pulses. Note within that context that control of filamentation processes in liquids and gases has been recently demonstrated by applying adaptive femtosecond pulse shaping techniques [27–29]. In our case, the power of our laser pulses amounts to a few MW and is three orders of magnitude below the critical power for self-focusing in air [30] being in the few GW regime. Recent advances in numerical simulations can calculate the interplay between propagation and material interaction as well as hydrodynamic effects [31]. It would be beneficial to combine these approaches taking into account specifically shaped laser pulses.

4 Conclusions

Our experiments reveal that temporally asymmetric femtosecond pulses applied to single shot surface structuring of fused silica via a 0.5NA microscope objective lead to two jointly associated results. On the one hand, from differences in the damage threshold energy with respect to an asymmetric pulse and its time reversed counterpart we conclude that multi-photon ionization and avalanche ionization are addressed in a different fashion. On the other hand, both pulse shapes lead to structures up to an order of magnitude below the diffraction limit. Moreover, these nanoscale structures remain by a factor of five below the diffraction limit during doubling the fluence. We believe that our approach shows a way to develop tailored pulse shapes for controlled nanoscale laser processing of dielectrics.

Acknowledgements This work was supported by the DFG via SPP 1139. L.E. and L.H. thank the DYNA program of ESF for travel support to COLA 2007.

References

1. L. Sudrie, A. Couairon, M. Franco, B. Lamouroux, B. Prade, S. Tzortzakis, A. Mysyrowicz, Phys. Rev. Lett. **89**, 186601 (2002)
2. A. Vogel, V. Venugopalan, Chem. Rev. **103**, 577 (2003)
3. F. Dausinger, F. Lichtner, H. Lubatschowski, *Femtosecond Technology for Technical and Medical Applications* (Springer, Berlin, 2004)
4. S.S. Mao, F. Quéré, S. Guizard, X. Mao, R.E. Russo, G. Petite, P. Martin, Appl. Phys. A **79**, 1695 (2004)
5. H. Misawa, J. Juodkazis, *3D Laser Microfabrication* (Wiley–VCH, Weinheim, 2006)

6. B.C. Stuart, M.D. Feit, A.M. Rubenchik, B.W. Shore, M.D. Perry, Phys. Rev. Lett. **74**, 2248 (1995)
7. M. Lenzner, J. Krüger, S. Sartania, Z. Cheng, C. Spielmann, G. Mourou, W. Kautek, F. Krausz, Phys. Rev. Lett. **80**, 4076 (1998)
8. A.C. Tien, S. Backus, H.C. Kapteyn, M.M. Murnane, G. Mourou, Phys. Rev. Lett. **82**, 3883 (1999)
9. M. Li, S. Menon, J.P. Nibarger, G.N. Gibson, Phys. Rev. Lett. **82**, 2394 (1999)
10. G. Petite, S. Guizard, P. Martin, F. Quéré, Phys. Rev. Lett. **83**, 5182 (1999)
11. Y.P. Deng, X.H. Xie, H. Xiong, Y.X. Leng, C.F. Cheng, H.H. Lu, R.X. Li, Z.Z. Xu, Opt. Express **13**, 3096 (2005)
12. R. Stoian, M. Boyle, A. Thoss, A. Rosenfeld, G. Korn, I.V. Hertel, Appl. Phys. A **77**, 265 (2003)
13. M. Wollenhaupt, A. Präkelt, C. Sarpe-Tudoran, D. Liese, T. Bayer, T. Baumert, Phys. Rev. A **73**, 063409 (2006)
14. A.M. Weiner, Rev. Sci. Instrum. **71**, 1929 (2000)
15. A. Präkelt, M. Wollenhaupt, A. Assion, Ch. Horn, C. Sarpe-Tudoran, M. Winter, T. Baumert, Rev. Sci. Instrum. **74**, 4950 (2003)
16. J.D. McMullen, J. Opt. Soc. Am. **67**, 1575 (1977)
17. M. Wollenhaupt, A. Assion, T. Baumert, in *Handbook of Lasers and Optics*, ed. by F. Träger (Springer, New York, 2007), chap. 12
18. M. Martínez-Corral, Proc. SPIE **5182**, 112 (2003)
19. L. Englert, B. Rethfeld, L. Haag, M. Wollenhaupt, C. Sarpe-Tudoran, T. Baumert, Opt. Express **15**, 17855 (2007)
20. J.M. Lui, Opt. Lett. **7**, 196 (1982)
21. A.P. Joglekar, H. Liu, G.J. Spooner, E. Meyhöfer, G. Mourou, A.J. Hunt, Appl. Phys. B **77**, 25 (2003)
22. M. Merano, G. Boyer, A. Trisorio, G. Chériaux, G. Mourou, Opt. Lett. **32**, 2239 (2007)
23. P. Audebert, Ph. Daguzan, A. Dos Santos, J.C. Gauthier, J.P. Geindre, S. Guizard, G. Hamoniaux, K. Krastev, P. Martin, G. Petite, A. Antonetti, Phys. Rev. Lett. **73**, 1990 (1994)
24. V.V. Temnov, K. Sokolowski-Tinten, P. Zhou, A. El-Khamhawy, D. von der Linde, Phys. Rev. Lett. **97**, 237403 (2006)
25. C. Sarpe-Tudoran, A. Assion, M. Wollenhaupt, M. Winter, T. Baumert, Appl. Phys. Lett. **88**, 261109 (2006)
26. B. Rethfeld, Phys. Rev. Lett. **92**, 187401 (2004)
27. G. Heck, J. Sloss, R.J. Levis, Opt. Commun. **259**, 216 (2006)
28. R. Ackermann, E. Salmon, N. Lascoux, J. Kasparian, P. Rohwetter, K. Stelmaszczyk, S. Li, A. Lindinger, L. Wöste, P. Béjot, L. Bonacina, J.-P. Wolf, Appl. Phys. Lett. **89**, 171117 (2006)
29. M.Y. Shverdin, S.N. Goda, G.Y. Yin, S.E. Harris, Opt. Lett. **31**, 1331 (2006)
30. W. Lui, S.L. Chin, Opt. Express **13**, 5750 (2005)
31. L. Hallo, A. Bourgeade, V.T. Tikhonchuk, C. Mezel, J. Breil, Phys. Rev. B **76**, 024101 (2007)